

Record High Magnetic Anisotropy in Three-Coordinate Mn^{III} and Cr^{II} Complexes: A Theoretical Perspective

Arup Sarkar, Reshma Jose, Harshit Ghosh, and Gopalan Rajaraman*

Cite This: *Inorg. Chem.* 2021, 60, 9680–9687

Read Online

ACCESS |

Metrics & More

Article Recommendations

Supporting Information

ABSTRACT: *Ab initio* calculations performed in two three-coordinate complexes [Mn{N(SiMe₃)₂}₃] (1) and [K(18-crown-6)(Et₂O)₂][Cr{N(SiMe₃)₂}₃] (2) reveal record-high magnetic anisotropy with the *D* values −64 and −15 cm^{−1}, respectively, enlisting *d*⁴ ions back in the race for single-ion magnets. A detailed spin-vibrational analysis performed of 1 and 2 suggests dominance under barrier relaxation due to the flexible coordination spheres around the metal ion. Furthermore, several *in silico* models were constructed by varying the nature of donor atoms based on the X-ray structure of 1 and 2, unveiling much larger anisotropy and robust single-ion magnet (SIM) characteristics for some of the models offering design clues for low-coordinate transition-metal SIMs.



1. INTRODUCTION

Single-molecule magnets (SMMs) have become a fascinating research area as this class of molecules exhibits magnetization just like permanent magnets below a critical temperature defined as blocking temperature T_B .¹ An important parameter associated with the blocking temperature is the barrier height for magnetization reversal (U_{eff}), which is correlated to the magnetic moment of different microstates and the nature of magnetic anisotropy. While in lanthanide complexes, the first-order spin-orbit coupling (SOC) is strong enough to produce large barrier heights,² in transition-metal (TM) systems, SOC is generally weak. This leads to relatively smaller anisotropy and smaller axial zero-field splitting (ZFS) parameter (*D*), the sign and magnitude of which can be fine-tuned using the ligand field.³

There are several challenges in enhancing the blocking temperature T_B in SMMs as several relaxation mechanisms other than the Orbach process spoil the direct correlation of T_B to U_{eff} values. Among others, quantum tunneling of magnetization (QTM) and spin-phonon/vibrational-mode relaxation mechanisms are a prominent source of relaxation, as shown in recent years by various groups.⁴ Earlier research in the SMM area focused on increasing the total spin (*S*) of the complexes by increasing the number of metal centers. After the discovery of a very small U_{eff} barrier in {Mn₁₉} clusters possessing record-high ground-state *S* value, it becomes clear that increasing the number of metal centers or the *S* value diminishes the axial anisotropy (*D* term), as evident from the equation proposed originally by Abragam and Bleaney⁵ and adapted in *ab initio* calculations later on. For this reason, mononuclear TM complexes gained significant attention,

leading to the birth of several single-ion magnets (SIMs) based on the low coordination number such as Fe(II/I), Ni(II), and Co(II), exhibiting very large U_{eff} values.⁶

In the early years of SMMs, the focus has been on TM cluster, particularly that of Mn(III) ions, as this offers an easy source of a negative *D* parameter for the chemists and unearthed numerous SMMs, albeit with smaller U_{eff}/T_B values.^{1a,7} The Mn(III) ions are very robust and can be easily incorporated in cluster aggregation and are relatively redox stable^{6a} but exhibit only small *D* values of the order of $\sim|5|$ cm^{−1}.⁸ While several low-coordinate TM ions were pursued recently for potential SMMs, Mn(III) has not been studied in detail, perhaps due to the perception that the expected *D* values are rather small.⁸ Apart from U_{eff} values, the blocking temperature is an important criterion, which is often very small for TM SMMs. This suggests that apart from the QTM effect, spin-vibrational relaxations are at play in such systems.⁴ How these effects manifest in these complexes is not fully understood.

To ascertain complexes that exhibit large negative *D* values and correlate the relaxation mechanism to spin-vibrational coupling, we performed multireference *ab initio* calculations using the ORCA suite.⁹ Here, we have studied in detail two

Received: March 30, 2021

Published: June 23, 2021

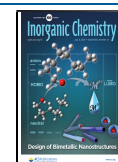
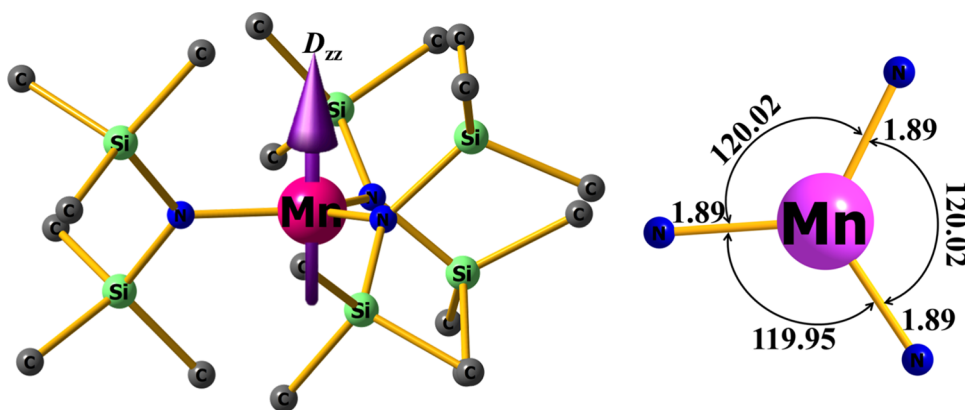


Table 1. Comparison of the ZFS Parameters Using Different Multireference Methods with Varying Numbers of Triplet and Singlet States on 1 and 2

complexes	method (+EHA)	quintet roots	triplet roots	singlet roots	D (cm^{-1})	E/D
1	SA-CASSCF	5	45		-64.3	0.0002
	NEVPT2	5	35		-64.5	0.0002
	NEVPT2	5	45		-64.3	0.0003
	NEVPT2	5	45	50	-63.1	0.0003
	DCD-CAS(2)	5	45		-63.7	0.0004
	QD-NEVPT2	5	45		-76.5	0.032
2	SA-CASSCF	5	45		-15.1	0.003
	NEVPT2	5	35		-15.2	0.003
	NEVPT2	5	45		-15.1	0.003
	NEVPT2	5	45	50	-14.6	0.003
	DCD-CAS(2)	5	45		-15.1	0.002
	QD-NEVPT2	5	45		-15.0	0.001

**Figure 1.** NEVPT2-computed D_{zz} axis of the molecule plotted on the X-ray structure (left) and three Mn–N bond lengths (in Å) and \angle N–Mn–N angles ($^\circ$) shown on the molecule (right). Color code: Mn: pink, N: blue, Si: light green, C: dark gray. Hydrogen is omitted for clarity.

three-coordinate d^4 systems, Mn(III) and Cr(II): $[\text{Mn}\{\text{N}(\text{SiMe}_3)_2\}_3]^{10}$ (1) and $[\text{K}(18\text{-crown-6})(\text{Et}_2\text{O})_2][\text{Cr}\{\text{N}(\text{SiMe}_3)_2\}_3]^{11}$ (2), using their reported X-ray structure. Our NEVPT2 calculations yield a record axial D value of -64 and -15 cm^{-1} for 1 and 2, respectively, with a negligible E/D value. The D value computed for both complexes is larger than any examples reported to date and suggests a potential SMM characteristic for these robust building block metal ions.

2. COMPUTATIONAL DETAILS

All the *ab initio* single-point calculations have been performed using the ORCA 4.1.0 program.⁹ The Douglas–Kroll–Hess (DKH) Hamiltonian was used to account for the scalar relativistic effect. DKH-contracted versions of the basis sets were used during the calculations—DKH-def2-TZVP for Mn, Cr, and Si, DKH-def2-TZVP(-f) for N, and DKH-def2-SVP for the rest of the atoms. During the orbital optimization step in the state-averaged complete active space self-consistent field (SA-CASSCF) method, 4 metal electrons in 5 metal d -orbitals were taken into consideration and optimized with 5 quintet and 35 triplet roots for Mn(III) and Cr(II) metal centers. Additional calculations have also been carried out with 5 quintets, 45 triplets, and 50 singlet states to check the effect of high-lying excited states on the spin–Hamiltonian (SH) parameters. The addition of extra 10 triplet roots and 50 singlet roots marginally affects the SH parameters (see Table 1). Strongly contracted N -electron valence perturbation theory second-order (NEVPT2) calculations have also been performed on the top of converged SA-CASSCF wave function to

include the dynamic electron correlation.¹² Additionally, the multistate dynamic correlation methods, such as second-order dynamical correlation-dressed complete active space (DCD-CAS(2))¹³ and quasi-degenerate N -electron valence-state perturbation theory second-order (QD-NEVPT2),¹⁴ were also performed to understand their effects in the estimation of D values. Spin–orbit interaction was accounted with the quasi-degenerate perturbation theory (QDPT) approach using the spin–orbit mean field (SOMF) operator. Only spin–orbit contributions toward ZFS were computed, and the SH parameters were determined from effective Hamiltonian approach (EHA) formalism.¹⁵ *Ab initio* ligand field theory (ALLFT) analysis has also been carried out to obtain very accurate d -orbital energies of the studied complexes.¹⁶

Geometry optimization and single-point frequency calculations have been carried out in the Gaussian 09 (Rev. D.01) program.¹⁷ The hybrid unrestricted B3LYP-D2 functional was used for the DFT calculations along with Ahlrich's triple- ζ valence polarized (TZVP) basis set for Mn, Cr, Si, and N and Ahlrich's split valence polarized (SVP) basis set for rest of the atoms.¹⁸

Furthermore, geometry optimization and subsequent vibrational analysis on the lattice unit cell calculations were carried out using periodic density functional methods implemented in the CP2K 6.1. suite with the N–M–N angles fixed to avoid deviation from the ideal symmetry.¹⁹ The Perdew–Burke–Ernzerhof (PBE)²⁰ gradient-corrected, generalized gradient approximation was used to describe the exchange–correlation functional and DZVP-MOLOPT-GTH (valence double zeta

(ζ) plus polarization, Goedecker–Teter–Hutter) basis set for atoms (H, C, and N) and DZVP-MOLOPT-SR-GTH for Cr and Mn atoms were used. The kinetic energy cutoff of 400 Ry was used with the Gaussian augmented plane-wave (GAPW) approach.²¹ The Grimme's D2 correction (DFT-D2) was used to account for the dispersion interactions. The boundary condition $a = b = c$ was set according to the crystallographic information file available. The Molden software was used for the visualization of the vibrational frequencies with a scale factor of 0.3.

3. RESULTS AND DISCUSSION

Complex **1** possesses a perfect D_{3h} symmetry as the three $\angle\text{N–Mn–N}$ bond angles are 120.02, 120.02, and 119.95° and the three Mn–N bond lengths are 1.89, 1.89, and 1.89 (in Å unit). It was also noticed that the $\{\text{MnN}_3\}$ core was planar, and the bulky trimethylsilyl groups surrounding the central moiety stabilize the low-coordinate molecule from further coordination *via* steric arrangements (see Figure 1). The NEVPT2-QDPT-calculated major anisotropy axes, that is, D_{zz} and g_{zz} axes, were found to be exactly perpendicular to the Mn–N₃ plane, that is, exactly collinear with the C_3 axis, which describes the axial nature of anisotropy present in the molecule.

3.1. ZFS Calculations. A record axial ZFS was found for this complex, showing a D value of -64 cm^{-1} with E/D estimated to be 0.0003, indicating strong easy-axis type anisotropy (see Table 1) for complex **1**. A very similar geometry was observed in the Cr(II) analogue, and the $\angle\text{N–Cr–N}$ bond angles (123.9, 115.81, and 120.29°) are not exactly similar and significantly deviated from D_{3h} symmetry. For complex **2**, the E/D value is estimated to be 0.003, which is 10 times larger than complex **1** (see Figure S1 and Table 1). The inclusion of higher-lying singlet excited states alters the D parameter marginally, and the changes are within $\sim 1\text{ cm}^{-1}$. Additionally, we have computed the ZFS parameters considering multistate multireference perturbation theory approaches such as DCD-CAS(2) and QD-NEVPT2 methods, followed by spin–orbit Hamiltonian (see Table 1). Unlike single-state NEVPT2 calculations, these multistate methods allow the CAS part of the wave function to relax. The D and E/D values for both the complexes are nearly unaltered due to the inclusion of state mixing, except for the QD-NEVPT2 method for **1**, in which the D value estimate is slightly larger. Thus, all the multireference methods suggest large negative D values with very small E/D values for both the complexes (see Table 1). It is also interesting to note that the D value obtained for both the complexes at the SA-CASSCF level of theory is close to the value obtained after multireference perturbation correction. This is attributed to the energy of the first excited quintet state, which contributes 97% to the net D value (see Tables S1 and S2 in the Supporting Information), suggesting negligible contribution due to incorporation of dynamic correlation.

The ground-state electronic configuration of complex **1** is $(d_z^2)^1(d_{yz})^1(d_{xz})^1(d_{xy})^1(d_{x^2-y^2})^0$, and this comprises 77% of the overall wave function. The major contribution (-62 cm^{-1}) toward the negative D value arises from the first excited state, which consists of $d_{xy} \rightarrow d_{x^2-y^2}$ (same M_L valued) electronic excitation, and this excited state contributes $\sim 97\%$ of the overall D value (see Figure 2 and Table S3 in ESI). Other electronic transitions were found to contribute negligibly to the overall D value. A very close analysis of the NEVPT2 states reveals that the first excited quintet state is only 19 cm^{-1} apart

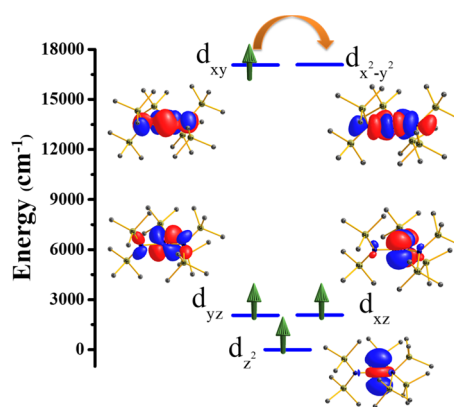


Figure 2. NEVPT2-LFT d -orbital diagram of complex **1**. The orange arrow indicates the first excited spin-allowed transition.

from the ground state and consequently results in a very strong second-order SOC. While the first excited state is the spin-allowed quintet, the second, third, and fourth excited states arise from the spin-flipped triplet transitions. These three excited states consist of a mixture of $d_{xy} \rightarrow d_{xz}/d_{yz}$ and $d_{xy} \rightarrow d_z^2$ transitions (see Table S3 in the Supporting Information). The computed g_x , g_y , and g_z values are 1.67, 1.67, and 1.14, respectively, for true spin $S = 2$ and 0.00, 0.00, and 5.14, respectively, for pseudospin $\hat{S} = 1/2$ manifold. In the case of complex **2**, the first excited state contributes 96% (-14.4 cm^{-1}) towards the overall D value. Again, the D value is negative due to the coupling with the prominent first excited state involving the same M_L level $d_{xy} \rightarrow d_{x^2-y^2}$ electronic excitation (see Figure S2 in the Supporting Information). Here, one major difference of complex **2** from complex **1** is that due to significant distortion from D_{3h} and the lower ligand field of Cr(II), the first excited state is 756 cm^{-1} apart, and the next three excited states are quintets (see Table S4). The computed g_x , g_y , and g_z values are 1.97, 1.97, and 1.58, respectively, for true spin $S = 2$ and 0.00, 0.00, and 6.351, respectively, for pseudospin $\hat{S} = 1/2$ manifold. We analyzed the NEVPT2 transition energies for quintet excited states for these two complexes and compared them with the experimental absorption spectra reported. The NEVPT2 calculations show two absorption bands at $18,930$ and $21,430\text{ cm}^{-1}$ for ${}^5E' \rightarrow {}^5E''$ and ${}^5E' \rightarrow {}^5A_1'$ transitions, respectively, for complex **1**. This is in agreement with the experimental values of $17,600$ and $21,280\text{ cm}^{-1}$ reported.¹⁰ For complex **2**, these two bands shift to $10,808\text{ cm}^{-1}$ (925 nm) and $12,855\text{ cm}^{-1}$ (778 nm), which is also in agreement with a broad feature observed at $12,135\text{ cm}^{-1}$.¹¹

In the case of non-Kramers ions like in these two cases studied, the tunnel splitting (Δ_{tun}) is generally larger, leading to faster relaxation *via* the QTM process. The tunnel splitting strongly depends on the local symmetry and ligand field environment around the metal ion. The high symmetry present in complexes **1** and **2** leads to smaller tunnel splitting (see Figure S3 and Table S5 in the Supporting Information). The first excited pseudo-KDs are separated by 154 cm^{-1} in the case of complex **1** and 45 cm^{-1} in the case of complex **2**. The multideterminant nature of the ground state leads to the mixing of the $|+2\rangle$ and $|-2\rangle$ states, and this is very prominent in complex **1** compared to **2** (see Table S5).

3.2. Spin-Vibrational Studies. The static electronic picture is insufficient to describe the relaxation mechanism or the spin dynamics of the system. Recent reports of spin-

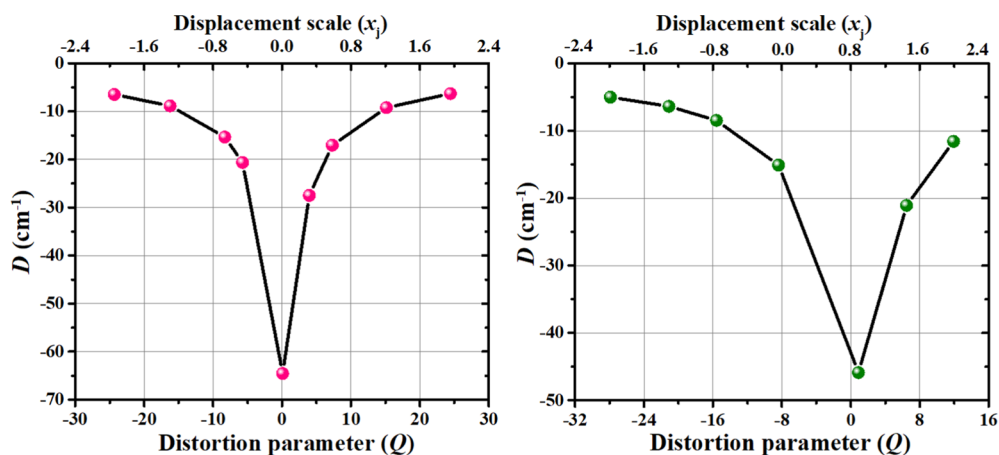


Figure 3. Variation of D values in complexes **1** (left) and **2** (right) with respect to the distortion parameter Q and displacement factor x_j for the ν_4 vibrational mode.

vibronic coupling that describe the role of vibrational frequencies of a single molecule or of the surrounding lattice are very important to elucidate the dynamic scenario of SMMs.⁴ In this regard, we have attempted to investigate the role of molecular vibrations occurring at low temperatures on the spin-orbit or M_s levels in the two complexes. Therefore, we have performed frequency calculations (normal modes) on the X-ray structures of **1** and **2** using density functional theory (DFT) methods (B3LYP-D2/TZVP, a similar vibrational pattern was also found for the optimized geometries; see Table S6 in the Supporting Information). Furthermore, attempts have also been made to analyze the frequencies arising from lattice unit cells of complexes **1** and **2** using periodic DFT calculations. The lattice vibrations computed on the optimized geometries were subjected to subsequent CASSCF/NEVPT2 calculations at lower-energy frequency points found at 247 and 429 cm^{-1} for **1** and 490 and 625 cm^{-1} for complex **2** (see Tables S7 and S8). Our calculations reveal that the lower-energy vibrations of the unit cells do not distort the core of the complexes and are rather associated with C–H bending modes of the SiMe_3 groups. Thus, CASSCF/NEVPT2 calculations on the lower energy vibrational points were found not to affect the ZFS parameters significantly. The computed D parameter complex **1** remains within the range of -53 to -64 cm^{-1} , and the D parameter almost remains constant for complex **2** (see Table S7 and Figure S4).

In the next step, local molecular vibrations were carefully analyzed, and five lower-energy vibrational modes below 80 cm^{-1} were examined, and these are ν_1 45.1 (40.1), ν_2 45.8(46.2), ν_3 58.4(50.3), ν_4 70.3(58.8), and ν_5 72.9 (69.9) for complex **1** (**2**) (see Figure S5 in the Supporting Information and animated GIF files). Out of the five vibrations mentioned, the ν_4 and ν_5 vibrations were found to be infrared-active and also broke the D_{3h} symmetry (see Figure S5). Here, ν_4 corresponds to $\angle\text{N–M–N}$ bond angle bending and correlates with Jahn–Teller active vibration (E' irreducible representation in D_{3h} symmetry). ν_5 corresponds to the out-of-plane (M–N–N–N) bending vibration of the metal ion and associated with A_2'' irreducible representation. Several displacement points in ν_4 and ν_5 vibrational surfaces were considered for CASSCF/NEVPT2 calculations. The maximum displacement scale of a particular vibration j , denoted by x_j , was fixed at 2.0 for both the complexes, as suggested earlier (see Tables S9 and S10 in the Supporting Information).²²

An angular distortion parameter Q was introduced, which is a sum of deviation from 120° from each of the equatorial $\angle\text{N–M–N}$ angles (denoted as α) (see Tables S9 and S10).^{6c} Here, in order to find out the spin-vibronic coupling, the variation in D and E/D has been computed with respect to the displacement of nuclear coordinates (x) using the following Hamiltonian²³

$$\hat{H}_{s\text{-vib}} = \left(\frac{\partial D}{\partial x} \right)_0 x \left[\hat{S}_Z^2 - \frac{S(S+1)}{3} \right] + \left(\frac{\partial E}{\partial x} \right)_0 x (\hat{S}_x^2 - \hat{S}_y^2) \quad (1)$$

In Figure 3, we plot computed D values with respect to Q and x_j , and these plots show that as the Q diverges from zero, the magnitude of D decreases for ν_4 vibrations (see Figure S6 in the Supporting Information). This is because an increase in Q disrupts the D_{3h} symmetry and, consequently, increases the gap between the d_{xy} and $d_{x^2-y^2}$ orbitals (see Figure 4). In complex **1**, the X-ray structure shows the highest negative D value and minimum E/D value (see Fig. S6) at equilibrium geometry or the zero displacement point, but for complex **2**, the X-ray structure significantly deviates from the ideal D_{3h} symmetry and therefore does not have the largest negative D or the lowest E/D at the zero displacement point. In complex **2**, at $x_j = 0.8$ (see Figure 3), the Q parameter shows a minimum and predicts a D value as high as -46 cm^{-1} .

Furthermore, we have developed a two-dimensional contour surface plot of magneto–structural correlation to see the effect of angle change on the D values for complexes **1** and **2** (see Figure 5). It is very clear that D is maximum when all the three equatorial angles are 120° . For **1**, the variation in D values is found to be relatively smaller for ν_5 vibrations compared to ν_4 modes (see Tables S11 and S12 in the Supporting Information). For complex **2**, no spin-vibronic coupling is detected as a much smaller change in D is noted. To rationalize this observation, the AILFT-computed d -orbitals are plotted, and this reveals that the $d_{xy} - d_{x^2-y^2}$ orbital energy gap is altered only slightly in **1** and negligibly in **2** (see Fig. S7–S8). A minute change in the $d_{xy} - d_{x^2-y^2}$ orbital gap alters the D value significantly in complex **1** and slightly in complex **2**. For complex **2**, ν_5 vibration not only alters the out-of-plane movement of Cr but also changes the equatorial angle simultaneously and thus raises the D value to a small extent relative to the equilibrium geometry.

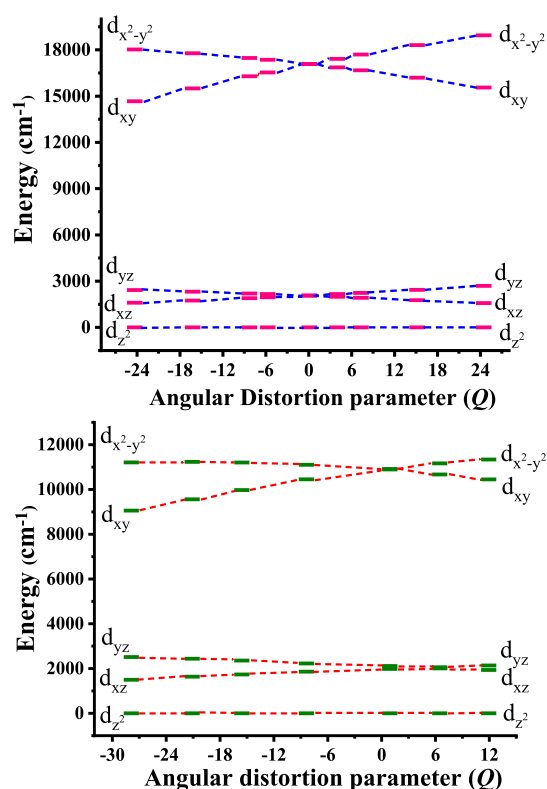


Figure 4. Variation of AILFT d -orbital energies with respect to the Q parameter for complex 1 (top) and for complex 2 (bottom) in ν_4 vibration.

In order to understand the slow relaxation of magnetization, quantum tunneling (or tunnel splitting) is an important factor. The spin-orbit energies of the M_S levels have been plotted against the displacement parameter to understand the variation of the tunnel splitting (Δ_{tun}) with respect to ν_4 and ν_5 vibrational modes. It revealed that the Δ_{tun} for $M_S = \pm 2$ states remain small and constant in ν_4 and ν_5 modes for both the complexes (see Figures S9 and S10). However, the Δ_{tun} between the $M_S = \pm 1$ level is equal to $6E$ and gives a direct measurement of the rhombicity present in the system. This value is minimum at $x_j = 0$ for complex 1 and $x_j = 0.8$ for complex 2.

The obtained result suggests that the ν_4 vibrational mode is dominant in controlling the magnetic anisotropy in trigonal planar d^4 systems, and this vibration likely offers a smaller barrier height for relaxation at lower temperatures. Between complexes 1 and 2, the spin-vibronic coupling is found to be stronger in the former.

At the equilibrium geometries, neglecting other effects, the computed U_{cal} values for complexes 1 and 2 are 153.8 and 44.7 cm^{-1} , respectively. Considering the vibrational relaxation ν_4 modes at the displacement scale of $x_j = \pm 2$, the U_{eff} value is expected to diminish to 19 and 15 cm^{-1} for complexes 1 and 2, respectively (neglecting the QTM effects) as depicted in Figure S9 (in the Supporting Information). This is substantially smaller than the barrier height estimated from the Orbach process and suggests a dominant spin-vibronic relaxation role in the magnetization relaxation in these complexes. This may be attributed to the fact that the $\angle\text{N-M-N}$ bond angle bending vibration is very subtle and does not require significant energy for structural distortion, and is strongly correlated with the d_{xy} and $d_{x^2-y^2}$ gap, altering the

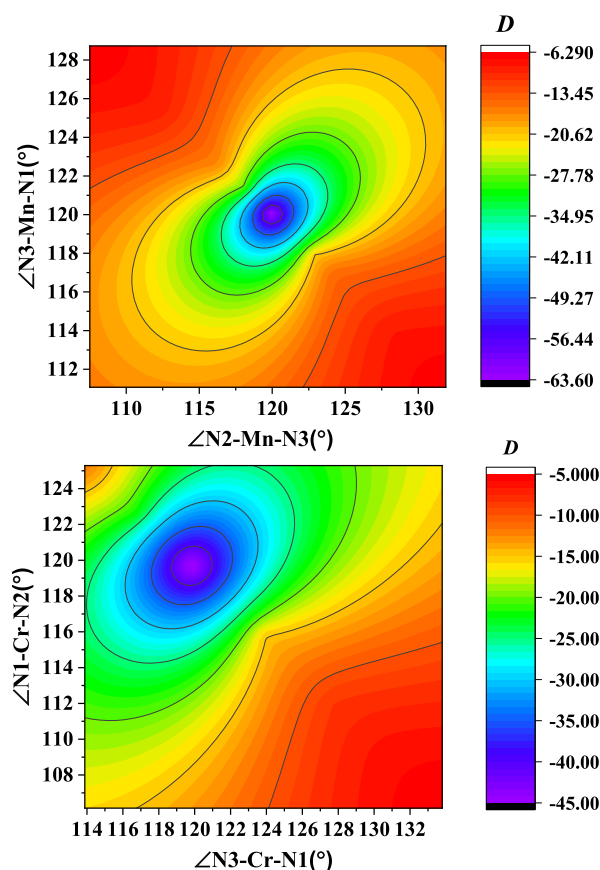


Figure 5. Contour surface plot of magneto-structural correlation of D obtained from the ν_4 mode for complex 1 (top) and for complex 2 (bottom).

magnetic anisotropy. This advocates a design principle that a rigid structure with a robust N-Mn-N angle could block such relaxation. An appropriate rigid ligand design or incorporation of a $\{\text{MnN}_3\}$ unit in a fullerene cage could hence be advantageous.

3.3. Role of Donor Atoms in the Estimation of D Values. We now switch our attention toward the effect of donor atoms in the magnetic anisotropy of complexes 1 and 2. To explore the effect of donor atoms in D values, six models 1a-c and 2a-c are designed (see Figure 6). Here, we have varied the donor atoms from carbon- $[\text{M}(\text{CH}_3)_3]$ (1a/2a) and nitrogen- $[\text{M}(\text{NH}_2)_3]$ (1b/2b), to oxygen- $[\text{M}(\text{OH})_3]$ (1c/2c) (where $M = \text{Mn}/\text{Cr}$) in order to understand their effect on the ZFS parameters. The models are designed in such a way that the core coordination environment of trigonal symmetry, which is crucial in the estimation of sign and strength of D value, is preserved.²⁸ The M-N bond lengths are the same compared to the parent complexes. For complexes 1a, 1c, 2a, and 2c, the M-X bond lengths were fixed at 1.965 Å (Mn-C),²⁴ 1.930 Å (Mn-O),²⁵ 2.140 Å (Cr-C),²⁶ and 2.09 Å (Cr-O)²⁷ as per the literature estimates.

The computed results have been summarized in Figures 6, S11, and Table S13 in the Supporting Information. To describe the nature of donor atoms, we have computed both the relativistic and nonrelativistic nephelauxetic reduction in B (Racah parameter) and SOC constant ζ of the model complexes from its free ion values (B_0 and ζ_0). The percentage reduction of B , that is, $(1 - B/B_0) \times 100\%$ and percentage reduction of ζ , that is, $(1 - \zeta/\zeta_0) \times 100\%$ serves as a reference

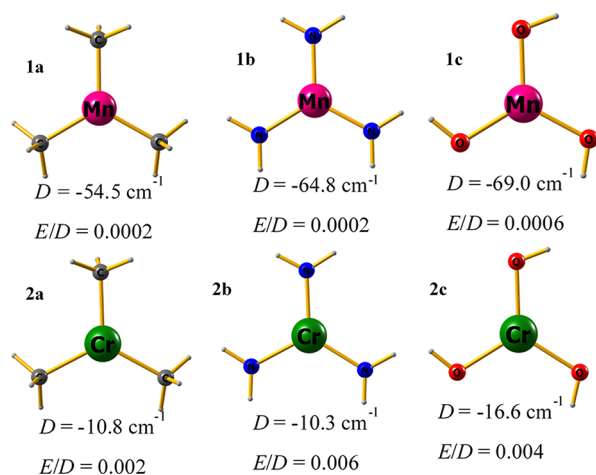


Figure 6. Various fictitious models developed by varying the donor atoms and their NEVPT2 computed ZFS parameters.

in the analysis of covalency present in the paramagnetic metal complexes.¹⁶ As the nephelauxetic reduction in B and ζ increases, the amount of the metal–ligand covalency is also expected to increase.

The D parameter for Mn(III) models is found to increase with the increase in hardness of the donor atoms in the following order: **1a** < **1b** < **1c** (see Table S13 in the Supporting Information). For Cr(II) model complexes, the D parameter is almost the same for C and N donor atoms but increases when O is the donor site; **2a** \approx **2b** < **2c**. Interestingly, the D value for model **1b** matches exactly with the parent complex **1** (X-ray structure). Unlike **1**, the NEVPT2 transition energies of complex **1b** show that the first four excited states are quintet in nature, and the first excited quintet is only 3.5 cm^{-1} apart (see Figure S11). This energy lowering of the first excited state does not enhance the ZFS as it is counterbalanced by enhancement of the Mn–N covalency in the model, as reflected in the reduction of B and ζ parameters). The nephelauxetic reduction in ζ and B in both the complexes suggests that hard donor OH^- reduces the metal–ligand covalency compared to the NH_2^- and CH_3^- groups. Thus, increasing hardness yields D values as high as -69 cm^{-1} for Mn(III) and -17 cm^{-1} for Cr(II) in trigonal planar geometry.

4. CONCLUSIONS

To the end, we have successfully employed an accurate *ab initio* method to explore the ZFS and ligand field parameters in two- Mn^{III} and Cr^{II} high-spin complexes. A record-high D value of -64 and -15 cm^{-1} was found for the X-ray structures of **1** and **2**, respectively. These two values are the highest known for any mononuclear d^4 systems (see also Table S14 in the Supporting Information).²⁹ While a significant barrier for magnetization relaxation is found for both the complexes, our detailed analysis revealed a strong spin–vibrational coupling in both complexes that are likely to yield smaller blocking temperatures. Studies on the model complexes suggest increasing hardness on the donor atom likely to enhance the magnetic anisotropy further in this class of molecules.

■ ASSOCIATED CONTENT

Supporting Information

The Supporting Information is available free of charge at <https://pubs.acs.org/doi/10.1021/acs.inorgchem.1c00978>.

Comparison of first two excitation energies of complexes **1** and **2** obtained from various multireference methods, major anisotropic axes plotted on complex **2** from the NEVPT2 level of theory, NEVPT2 vertical excitation spectrum, CASSCF electronic configuration, and their respective contribution toward D and E values for the ground state and six lower-lying excited states for complex **1** and four lower-lying excited states for complex **2**, NEVPT2-LFT d -orbital splitting diagram for complex **2**, energy profile diagram of the lowest five spin–orbit states of complex **1** and complex **2** obtained from the NEVPT2/QDPT/EHA method, wavefunction decomposition spin–orbit coupled states (M_s) of $S = 2$ manifold for complex **1** and **2**, selected structural parameters of the X-ray structure and DFT optimized geometries of complex **1** and **2**, single-point CASSCF/NEVPT2 calculations performed on the low-energy lattice unit cell vibrations for complexes **1** and **2**, low-energy vibrational IR spectra obtained from periodic DFT calculations on the lattice unit cells of complex **1** and complex **2**, DFT-computed IR spectrum of the two complexes at far-IR frequencies, variation of D and E/D values with respect to Q parameter along with their energies of the first excited state for complexes **1** and **2**, variation of E/D with respect to Q parameter and x_j for complex **1** and complex **2**, variation of D , E/D , first excited state NEVPT2 energy values with respect to the displacement of Mn along the z -direction for complex **1** and complex **2**, variation of *ab initio* LFT d -orbital splitting of complex **1** and complex **2**, variation of the energy of M_S levels with respect to different vibrational modes, *ab initio* computed ligand field and zero-field splitting parameters of the model and parent complexes, NEVPT2-computed transition energies of the model complexes with 5 quintet and 45 triplet states, and literature survey of all reported mononuclear high-spin Mn(III) and Cr(II) complexes (PDF)

Animated images of vibrational modes (ZIP)

■ AUTHOR INFORMATION

Corresponding Author

Gopalan Rajaraman – Department of Chemistry, Indian Institute of Technology Bombay, Mumbai 400076, Maharashtra, India; orcid.org/0000-0001-6133-3026; Email: rajaraman@chem.iitb.ac.in

Authors

Arup Sarkar – Department of Chemistry, Indian Institute of Technology Bombay, Mumbai 400076, Maharashtra, India
 Reshma Jose – Department of Chemistry, Indian Institute of Technology Bombay, Mumbai 400076, Maharashtra, India
 Harshit Ghosh – Department of Chemistry, Indian Institute of Technology Bombay, Mumbai 400076, Maharashtra, India

Complete contact information is available at:

<https://pubs.acs.org/doi/10.1021/acs.inorgchem.1c00978>

Author Contributions

The manuscript was written through the contributions of all authors. All authors have given approval to the final version of the manuscript.

Funding

This work was funded by the DST and SERB (CRG/2018/000430; DST/SJF/CSA-03/2018-10; SB/SJF/2019-20/12), UGC-UKIERI (184-1/2018(IC)), and SUPRA (SPR/2019/001145).

Notes

The authors declare no competing financial interest.

ACKNOWLEDGMENTS

R.J. thanks the DST-INSPIRE, and A.S. thanks the IIT Bombay for I-PDF funding.

REFERENCES

- (1) (a) Sessoli, R.; Gatteschi, D.; Caneschi, A.; Novak, M. A. Magnetic bistability in a metal-ion cluster. *Nature* **1993**, *365*, 141–143. (b) Gatteschi, D.; Sessoli, R.; Villain, J. *Molecular Nanomagnets*; Oxford University Press on Demand, 2006; Vol. 5.
- (2) Woodruff, D. N.; Winpenny, R. E. P.; Layfield, R. A. Lanthanide single-molecule magnets. *Chem. Rev.* **2013**, *113*, 5110–5148.
- (3) Gomez-Coca, S.; Cremades, E.; Aliaga-Alcalde, N.; Ruiz, E. Mononuclear single-molecule magnets: tailoring the magnetic anisotropy of first-row transition-metal complexes. *J. Am. Chem. Soc.* **2013**, *135*, 7010–7018.
- (4) (a) Gómez-Coca, S.; Urtizborea, A.; Cremades, E.; Alonso, P. J.; Camón, A.; Ruiz, E.; Luis, F. Origin of slow magnetic relaxation in Kramers ions with non-uniaxial anisotropy. *Nat. Commun.* **2014**, *5*, 4300. (b) Rechkemmer, Y.; Breitgoff, F. D.; van der Meer, M.; Atanasov, M.; Hakl, M.; Orlita, M.; Neugebauer, P.; Neese, F.; Sarkar, B.; van Slageren, J. A four-coordinate cobalt(II) single-ion magnet with coercivity and a very high energy barrier. *Nat. Commun.* **2016**, *7*, 10467. (c) Escalera-Moreno, L.; Suaud, N.; Gaita-Ariño, A.; Coronado, E. Determining Key Local Vibrations in the Relaxation of Molecular Spin Qubits and Single-Molecule Magnets. *J. Phys. Chem. Lett.* **2017**, *8*, 1695–1700. (d) Lunghi, A.; Totti, F.; Sessoli, R.; Sanvito, S. The role of anharmonic phonons in under-barrier spin relaxation of single molecule magnets. *Nat. Commun.* **2017**, *8*, 14620. (e) Moseley, D. H.; Stavretis, S. E.; Thirunavukkuarasu, K.; Ozerov, M.; Cheng, Y.; Daemen, L. L.; Ludwig, J.; Lu, Z.; Smirnov, D.; Brown, C. M.; Pandey, A.; Ramirez-Cuesta, A. J.; Lamb, A. C.; Atanasov, M.; Bill, E.; Neese, F.; Xue, Z.-L. Spin-phonon couplings in transition metal complexes with slow magnetic relaxation. *Nat. Commun.* **2018**, *9*, 2572. (f) Penfold, T. J.; Gindensperger, E.; Daniel, C.; Marian, C. M. Spin-vibronic mechanism for intersystem crossing. *Chem. Rev.* **2018**, *118*, 6975–7025.
- (5) Abragam, A.; Bleaney, B. *Electron Paramagnetic Resonance of Transition Ions*; OUP Oxford, 2012.
- (6) (a) Zadrozny, J. M.; Xiao, D. J.; Atanasov, M.; Long, G. J.; Grandjean, F.; Neese, F.; Long, J. R. Magnetic blocking in a linear iron(I) complex. *Nat. Chem.* **2013**, *5*, 577. (b) Zadrozny, J. M.; Atanasov, M.; Bryan, A. M.; Lin, C.-Y.; Rekker, B. D.; Power, P. P.; Neese, F.; Long, J. R. Slow magnetization dynamics in a series of two-coordinate iron(II) complexes. *Chem. Sci.* **2013**, *4*, 125–138. (c) Yao, X.-N.; Du, J.-Z.; Zhang, Y.-Q.; Leng, X.-B.; Yang, M.-W.; Jiang, S.-D.; Wang, Z.-X.; Ouyang, Z.-W.; Deng, L.; Wang, B.-W.; Gao, S. Two-Coordinate Co(II) Imido Complexes as Outstanding Single-Molecule Magnets. *J. Am. Chem. Soc.* **2016**, *139*, 373–380. (d) Bunting, P. C.; Atanasov, M.; Damgaard-Møller, E.; Perfetti, M.; Crassee, I.; Orlita, M.; Overgaard, J.; Van Slageren, J.; Neese, F.; Long, J. R. A linear cobalt(II) complex with maximal orbital angular momentum from a non-Aufbau ground state. *Science* **2018**, *362*, No. eaat7319. (e) Craig, G. A.; Sarkar, A.; Woodall, C. H.; Hay, M. A.; Marriott, K. E. R.; Kamenev, K. V.; Moggach, S. A.; Brechin, E. K.; Parsons, S.; Rajaraman, G.; Murrie, M. Probing the origin of the giant magnetic anisotropy in trigonal bipyramidal Ni(II) under high pressure. *Chem. Sci.* **2018**, *9*, 1551–1559. (f) Sarkar, A.; Dey, S.; Rajaraman, G. Role of Coordination Number and Geometry in Controlling the Magnetic Anisotropy in Fe II, Co II, and Ni II Single-Ion Magnets. *Chem.—Eur. J.* **2020**, *26*, 14036–14058.
- (7) Ako, A. M.; Hewitt, I. J.; Mereacre, V.; Clérac, R.; Wernsdorfer, W.; Anson, C. E.; Powell, A. K. A Ferromagnetically Coupled Mn19 Aggregate with a Record $S=83/2$ Ground Spin State. *Angew. Chem.* **2006**, *118*, 5048–5051.
- (8) (a) Maurice, R.; de Graaf, C.; Guihéry, N. Magnetostructural relations from a combined ab initio and ligand field analysis for the nonintuitive zero-field splitting in Mn(III) complexes. *J. Chem. Phys.* **2010**, *133*, 084307. (b) Ishikawa, R.; Miyamoto, R.; Nojiri, H.; Breedlove, B. K.; Yamashita, M. Slow Relaxation of the Magnetization of an Mn(III) Single Ion. *Inorg. Chem.* **2013**, *52*, 8300–8302. (c) Vallejo, J.; Pascual-Álvarez, A.; Cano, J.; Castro, I.; Julve, M.; Lloret, F.; Krzystek, J.; De Munno, G.; Armentano, D.; Wernsdorfer, W.; Ruiz-García, R.; Pardo, E. Field-induced hysteresis and quantum tunneling of the magnetization in a mononuclear manganese(III) complex. *Angew. Chem.* **2013**, *52*, 14075–14079. (d) Chen, L.; Wang, J.; Liu, Y.-Z.; Song, Y.; Chen, X.-T.; Zhang, Y.-Q.; Xue, Z.-L. Slow Magnetic Relaxation in Mononuclear Octahedral Manganese(III) Complexes with Dibenzoylemethanide Ligands. *Eur. J. Inorg. Chem.* **2015**, *2015*, 271–278. (e) Craig, G. A.; Marbey, J. J.; Hill, S.; Roubeau, O.; Parsons, S.; Murrie, M. Field-induced slow relaxation in a monometallic manganese(III) single-molecule magnet. *Inorg. Chem.* **2015**, *54*, 13–15. (f) Pascual-Álvarez, A.; Vallejo, J.; Pardo, E.; Julve, M.; Lloret, F.; Krzystek, J.; Armentano, D.; Wernsdorfer, W.; Cano, J. Field-Induced Slow Magnetic Relaxation in a Mononuclear Manganese(III)-Porphyrin Complex. *Chemistry* **2015**, *21*, 17299–17307. (g) Duboc, C. Determination and prediction of the magnetic anisotropy of Mn ions. *Chem. Soc. Rev.* **2016**, *45*, 5834–5847. (h) Realista, S.; Fitzpatrick, A. J.; Santos, G.; Ferreira, L. P.; Barroso, S.; Pereira, L. C. J.; Bandeira, N. A. G.; Neugebauer, P.; Hrubý, J.; Morgan, G. G.; van Slageren, J.; Calhorda, M. J.; Martinho, P. N. A Mn(III) single ion magnet with tridentate Schiff-base ligands. *Dalton Trans.* **2016**, *45*, 12301–12307. (i) Sanakis, Y.; Krzystek, J.; Maganas, D.; Grigoropoulos, A.; Ferentinos, E.; Kostakis, M. G.; Petroulea, V.; Pissas, M.; Thirunavukkuarasu, K.; Wernsdorfer, W.; Neese, F.; Kyritsis, P. Magnetic Properties and Electronic Structure of the $S = 2$ Complex $[Mn(III)\{(OPPh)_2N\}_3]$ Showing Field-Induced Slow Magnetization Relaxation. *Inorg. Chem.* **2020**, *59*, 13281–13294.
- (9) Neese, F. Software update: the ORCA program system, version 4.0. *WIRES: Comput. Mol. Sci.* **2018**, *8*, No. e1327.
- (10) Ellison, J. J.; Power, P. P.; Shoner, S. C. First examples of three-coordinate manganese(III) and cobalt(III): synthesis and characterization of the complexes $M[N(SiMe_3)_2]_3$ ($M = Mn$ or Co). *J. Am. Chem. Soc.* **1989**, *111*, 8044–8046.
- (11) Wagner, C. L.; Phan, N. A.; Fetting, J. C.; Berben, L. A.; Power, P. P. New Characterization of $V\{N(SiMe_3)_2\}_3$: Reductions of Tris[bis(trimethylsilyl)amido]vanadium(III) and -chromium(III) To Afford the Reduced Metal(II) Anions $[M\{N(SiMe_3)_2\}_3]^-$ ($M = V$ and Cr). *Inorg. Chem.* **2019**, *58*, 6095–6101.
- (12) Angeli, C.; Cimiraaglia, R.; Evangelisti, S.; Leininger, T.; Malrieu, J.-P. Introduction of off-electron valence states for multi-reference perturbation theory. *J. Chem. Phys.* **2001**, *114*, 10252–10264.
- (13) Lang, L.; Neese, F. Spin-dependent properties in the framework of the dynamic correlation dressed complete active space method. *J. Chem. Phys.* **2019**, *150*, 104104.
- (14) Angeli, C.; Borini, S.; Cestari, M.; Cimiraaglia, R. A quasidegenerate formulation of the second order n-electron valence state perturbation theory approach. *J. Chem. Phys.* **2004**, *121*, 4043–4049.
- (15) Maurice, R.; Bastardis, R.; Graaf, C. d.; Suaud, N.; Mallah, T.; Guihéry, N. Universal theoretical approach to extract anisotropic spin Hamiltonians. *J. Chem. Theory Comput.* **2009**, *5*, 2977–2984.
- (16) Singh, S. K.; Eng, J.; Atanasov, M.; Neese, F. Covalency and chemical bonding in transition metal complexes: An ab initio based ligand field perspective. *Coord. Chem. Rev.* **2017**, *344*, 2–25.
- (17) *Gaussian 09*, Revision D. 01; Frisch, M. J.; Trucks, G. W.; Schlegel, H. B.; Scuseria, G. E.; Robb, M. A.; Cheeseman, J. R.;

Scalmani, G.; Barone, V.; Mennucci, B.; Petersson, G. A.; et al. Gaussian, Inc.: Wallingford, CT, USA, 2013.

(18) (a) Schäfer, A.; Horn, H.; Ahlrichs, R. Fully optimized contracted Gaussian basis sets for atoms Li to Kr. *J. Chem. Phys.* **1992**, *97*, 2571–2577. (b) Schäfer, A.; Huber, C.; Ahlrichs, R. Fully optimized contracted Gaussian basis sets of triple zeta valence quality for atoms Li to Kr. *J. Chem. Phys.* **1994**, *100*, 5829–5835.

(19) Kühne, T. D.; Iannuzzi, M.; Del Ben, M.; Rybkin, V. V.; Seewald, P.; Stein, F.; Laino, T.; Khaliullin, R. Z.; Schütt, O.; Schiffmann, F.; Golze, D.; Wilhelm, J.; Chulkov, S.; Bani-Hashemian, M. H.; Weber, V.; Borstnik, U.; TAILLEFUMIER, M.; Jakobovits, A. S.; Lazzaro, A.; Pabst, H.; Müller, T.; Schade, R.; Guidon, M.; Andermatt, S.; Holmberg, N.; Schenter, G. K.; Hehn, A.; Bussy, A.; Belleflamme, F.; Tabacchi, G.; GlöB, A.; Lass, M.; Bethune, I.; Mundy, C. J.; Plessl, C.; Watkins, M.; VandeVondele, J.; Krack, M.; Hutter, J. CP2K: An electronic structure and molecular dynamics software package—Quickstep: Efficient and accurate electronic structure calculations. *J. Chem. Phys.* **2020**, *152*, 194103.

(20) Perdew, J. P.; Burke, K.; Ernzerhof, M. Generalized gradient approximation made simple. *Phys. Rev. Lett.* **1996**, *77*, 3865.

(21) Nabi, R.; Rajaraman, G. Deciphering the origin of variation in the spin ground state and oxidation state of a {Mn19} cluster on a Au(111) surface: is the Au(111) surface innocent? *Chem. Commun.* **2019**, *55*, 8238–8241.

(22) Goodwin, C. A. P.; Ortu, F.; Reta, D.; Chilton, N. F.; Mills, D. P. Molecular magnetic hysteresis at 60 kelvin in dysprosocenium. *Nature* **2017**, *548*, 439.

(23) Rechkemmer, Y.; Breitgoff, F. D.; Van Der Meer, M.; Atanasov, M.; Hakl, M.; Orlita, M.; Neugebauer, P.; Neese, F.; Sarkar, B.; Van Slageren, J. A four-coordinate cobalt (II) single-ion magnet with coercivity and a very high energy barrier. *Nat. Commun.* **2016**, *7*, 10467.

(24) Fernández, F. J.; Venkatesan, K.; Blacque, O.; Alfonso, M.; Schmalte, H. W.; Berke, H. Generation and Coupling of [Mn(dmpe)-2(CCR)(CC)]. Radicals Producing Redox-Active C4-Bridged Rigid-Rod Complexes. *Chem.—Eur. J.* **2003**, *9*, 6192–6206.

(25) Krzystek, J.; Yeagle, G. J.; Park, J.-H.; Britt, R. D.; Meisel, M. W.; Brunel, L.-C.; Telsler, J. High-Frequency and -Field EPR Spectroscopy of Tris(2,4-pentanedionato)manganese(III): Investigation of Solid-State versus Solution Jahn–Teller Effects. *Inorg. Chem.* **2003**, *42*, 4610–4618.

(26) Himmelbauer, D.; Stöger, B.; Veiros, L. F.; Pignitter, M.; Kirchner, K. Cr(II) and Cr(I) PCP Pincer Complexes: Synthesis, Structure, and Catalytic Reactivity. *Organometallics* **2019**, *38*, 4669–4678.

(27) (a) Deng, Y.-F.; Han, T.; Wang, Z.; Ouyang, Z.; Yin, B.; Zheng, Z.; Krzystek, J.; Zheng, Y.-Z. Uniaxial magnetic anisotropy of square-planar chromium(ii) complexes revealed by magnetic and HF-EPR studies. *Chem. Commun.* **2015**, *51*, 17688–17691. (b) Yousif, M.; Cabelof, A. C.; Martin, P. D.; Lord, R. L.; Groysman, S. Synthesis of a mononuclear, non-square-planar chromium(ii) bis(alkoxide) complex and its reactivity toward organic carbonyls and CO₂. *Dalton Trans.* **2016**, *45*, 9794–9804.

(28) Sarkar, A.; Tewary, S.; Sinkar, S.; Rajaraman, G. Magnetic Anisotropy in Co II X 4 (X=O, S, Se) Single-Ion Magnets: Role of Structural Distortions versus Heavy Atom Effect. *Chem.—Asian J.* **2019**, *14*, 4696–4704.

(29) Freitag, K.; Stennett, C. R.; Mansikkamäki, A.; Fischer, R. A.; Power, P. P. Two-Coordinate, Nonlinear Vanadium(II) and Chromium(II) Complexes of the Silylamide Ligand-N(SiMePh₂)₂: Characterization and Confirmation of Orbitaly Quenched Magnetic Moments in Complexes with Sub-d⁵ Electron Configurations. *Inorg. Chem.* **2021**, *60*, 4108–4115.